THE JOURNAL OF PHYSICAL CHEMISTRY A
A JOURNAL OF THE AMERICAN CHEMICAL SOCIETY

pubs.acs.org/JPCA

Article

Reaction Kinetics of CH_2OO and *syn*-CH_3CHOO Criegee Intermediates with Acetaldehyde

Published as part of The Journal of Physical Chemistry A virtual special issue "Xueming Yang Festschrift".

Haotian Jiang, Yue Liu, Chunlei Xiao, Xueming Yang, and Wenrui Dong*

Cite This: *J. Phys. Chem. A* 2024, 128, 4956−4965

Read Online

ACCESS | Metrics & More | Article Recommendations | Supporting Information

ABSTRACT: Criegee intermediates exert a crucial influence on atmospheric chemistry, functioning as powerful oxidants that facilitate the degradation of pollutants, and understanding their reaction kinetics is essential for accurate atmospheric modeling. In this study, the kinetics of CH_2OO and *syn*-CH_3CHOO reactions with acetaldehyde (CH_3CHO) were investigated using a flash photolysis reaction tube coupled with the OH laser-induced fluorescence (LIF) method. The experimental results indicate that the reaction of *syn*-CH_3CHOO with CH_3CHO is independent of pressure in the range of 5−50 Torr when using Ar as the bath gas. However, the rate coefficient for the reaction between CH_2OO and CH_3CHO at 5.5 Torr was found to be lower compared to the near-constant values observed between 10 and 100 Torr. Furthermore, the reaction of *syn*-CH_3CHOO with CH_3CHO demonstrated positive temperature dependence from 283 to 330 K, with a rate coefficient of $(2.11 \pm 0.45) \times 10^{-13}$ cm^3 molecule^{-1} s^{-1} at 298 K. The activation energy and pre-exponential factor derived from the Arrhenius plot for this reaction were determined to be 2.32 ± 0.49 kcal mol^{-1} and $(1.66 \pm 0.61) \times 10^{-11}$ cm^3 molecule^{-1} s^{-1}, respectively. In comparison, the reaction of CH_2OO with CH_3CHO exhibited negative temperature dependence, with a rate coefficient of $(2.16 \pm 0.39) \times 10^{-12}$ cm^3 molecule^{-1} s^{-1} at 100 Torr and 298 K and an activation energy and a pre-exponential factor of −1.73 ± 0.31 kcal mol^{-1} and $(1.15 \pm 0.21) \times 10^{-13}$ cm^3 molecule^{-1} s^{-1}, respectively, over the temperature range of 280−333 K.

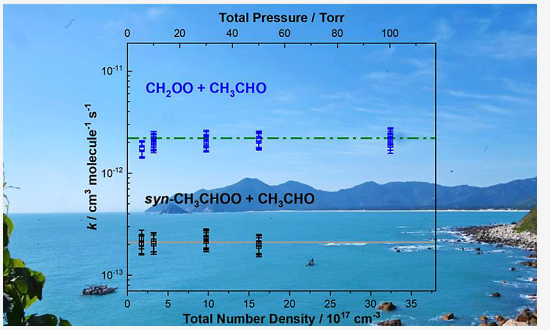

1. INTRODUCTION

The ozonolysis of alkenes in the gas phase occurs through the 1,3-cycloaddition mechanism, resulting in the formation of a cyclic primary ozonide (POZ). This unstable intermediate promptly decomposes into carbonyl oxide species, known as Criegee intermediates.[1] Due to the highly exothermic nature of this reaction, the Criegee intermediates (CIs) possess high internal energy. As a result, they can either undergo unimolecular decomposition, yielding products such as OH radicals or be stabilized through collisions with atmospheric bath gases, leading to the formation of stabilized Criegee intermediates (SCIs). These SCIs have a sufficiently long lifetime, enabling them to engage in bimolecular reactions with atmospheric species.

The simplest SCI, formaldehyde oxide (CH_2OO), is a major product from the ozonolysis of isoprene and other terminal or exocyclic alkenes. Its primary atmospheric sink is through reaction with water vapor, particularly water dimers.[2−5] The second smallest CI, CH_3CHOO, exists in two conformers that differ based on the orientation of the methyl group relative to the terminal oxygen atom. The unimolecular reaction of *anti*-CH_3CHOO is relatively slow[6,7] compared to its bimolecular reaction with water vapor and SO_2 under atmospheric conditions.[3,5,8−15] In contrast, the primary sink of *syn*-CH_3CHOO is through its unimolecular reaction, which predominantly generates OH radicals.[16,17]

Carbonyl compounds have been employed as scavengers for SCIs in various ozonolysis studies.[18] The reactions between SCIs and carbonyl compounds occur via a 1,3-cycloaddition mechanism, where the SCIs add across the C=O bond of carbonyl compounds.[19−24] It is worth noting that the carbonyl compounds exhibit significant reactivity toward numerous atmospheric oxidants. For instance, the rate coefficients for the reactions of acetaldehyde with OH and Cl at a temperature of 297 K have been reported to be approximately 1.5×10^{-11}[25−28] and 7.7×10^{-11} cm^3 molecule^{-1} s^{-1}, respectively.[29]

Acetaldehyde, one of the most abundant aldehydes in the atmosphere, is a crucial volatile organic compound (VOC). Acetaldehyde is frequently employed to represent aldehydes in atmospheric models. Notably, its atmospheric concentration is

Received: March 1, 2024
Revised: June 5, 2024
Accepted: June 5, 2024
Published: June 13, 2024

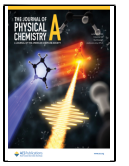

https://doi.org/10.1021/acs.jpca.4c01374
J. Phys. Chem. A 2024, 128, 4956−4965

comparable to that of formaldehyde, with observed concentration ratios of acetaldehyde to formaldehyde spanning from 0.4 to 1.4 at various rural, forested, and urban locations.[30] Several studies have investigated the reaction between CH_2OO and CH_3CHO. The reaction products of this reaction have been reported to be formaldehyde, formic acid, and acetic acid, as measured by photolysis/tunable synchrotron photoionization mass spectrometry.[31] The rate coefficient for this reaction was determined to be $(9.4 \pm 0.7) \times 10^{-13}$ cm^3 molecule^{-1} s^{-1} at 293 K and 4 Torr in helium.[31] By detecting the reaction product formaldehyde using the laser-induced fluorescence method, Stone et al. reported a rate coefficient of $(1.48 \pm 0.04) \times 10^{-12}$ cm^3 molecule^{-1} s^{-1} at 293 K and 25 Torr in nitrogen.[32] Employing the UV absorption method, Elsamra et al. observed that this reaction exhibits a negative temperature dependence between 298 and 494 K, with rate coefficients of $(1.1 \pm 0.1) \times 10^{-12}$ and $(1.2 \pm 0.2) \times 10^{-12}$ cm^3 molecule^{-1} s^{-1} at 298 K and 4 and 25 Torr, respectively.[33] The rate coefficient for the reaction of CH_3CHOO, derived from the ozonolysis of *trans*-2-butene, with CH_3CHO was measured to be $(1.1 \pm 0.4) \times 10^{-12}$ cm^3 molecule^{-1} s^{-1} in an atmospheric flow reactor using Fourier transform infrared spectroscopy.[34] However, the conformer-specific rate coefficient for this reaction has not been reported to date.

In this work, the kinetics of the following reactions are studied:

$$CH_2OO + CH_3CHO \xrightarrow{k_1} \text{Products} \quad (1)$$

$$syn\text{-}CH_3CHOO + CH_3CHO \xrightarrow{k_2} \text{Products} \quad (2)$$

The rate coefficients of reactions 1 and 2 were investigated as a function of temperature and pressure. The temperature range covered was from 283 to 333 K, while the pressure range extended from 5 to 100 Torr. The OH laser-induced fluorescence technique was employed to measure the rate coefficients under these varying conditions. Furthermore, the influence of bath gas on the rate coefficients of the CH_2OO + CH_3CHO reaction was examined and discussed.

2. EXPERIMENTAL SECTION

The current experiment was conducted using an apparatus previously described in our published work.[4,35] Briefly, aldehydes (1% in argon), oxygen (99.995%, DL Special Gases Co.), and the bath gas argon (99.999%, DL Special Gases Co.) were introduced into a premixing cell before entering the quartz tube reactor, with their flow rates regulated by calibrated mass flow controllers (MKS, GM50A Series). Argon, with its flow rate controlled, was bubbled through a bubble bottle to carry CH_2I_2 (99%, Macklin) vapor into the quartz reactor. The aldehyde concentrations were measured using the UV absorption method in a Herriott cell (40.1 cm in length), employing a UV−vis−NIR light source (DH-2000-S-DUV-TTL, Ocean Insight) and a spectrometer (Maya2000 Pro, Ocean Insight). The effective optical length of the cell is 850.9 ± 46.4 cm. The UV absorption spectrum of acetaldehyde is shown in Figure S1. The concentration of CH_2I_2 in the quartz reactor was measured with a deep UV LED (DUV325-H46, Roithner Lasertechnik, centered at 322.4 nm with an FWHM of 11 nm) and a balanced amplified photodetector (Thorlabs, PDB405A), based on the known absorption cross-section[36−38] and emission profile of the LED.

CH_2OO was produced by photolyzing CH_2I_2 in the presence of excess O_2 using a 355 nm laser, generated from the third harmonic generation of a Nd:YAG laser (Beamtech Nimma 900). For photolysis reactions, typical pulse energies of approximately 45 mJ/cm^2 were used for CH_2I_2 and 64 mJ/cm^2 for CH_3CHI_2. The 355 nm wavelength was chosen instead of 266 or 248 nm to prevent photodissociation of acetaldehyde by the photolysis laser. Following each photolysis laser pulse, the time-resolved intensity of OH radicals, resulting from the unimolecular reaction of CH_2OO, was detected using the laser-induced fluorescence method.

A probe laser with a wavelength of 282 nm was used to excite the OH radicals through the $P_1(1)$ line of the (1,0) band of the $A^2\Sigma^+ \leftarrow X^2\Pi$ transition. This probe laser was generated by frequency-doubling the output of a dye laser (Narrow Scan High Rep), which was pumped by the second harmonic of a Nd:YAG laser (Edgewave INNOSLAB: IS12II-ET, 10 kHz). The probe laser was positioned orthogonally to the photolysis laser at the center of the reaction zone. A delay generator (Stanford Research System, DG535) was employed to control the delay between the two laser pulses. The rapid vibrational relaxation of OH ($A^2\Sigma^+$ $\nu = 1$), approximately 4.3×10^5 s^{-1} at 10 Torr in an Ar bath gas,[39] results in the predominance of fluorescence emission in the (0, 0) vibronic band centered around 308 nm. The OH fluorescence was collected perpendicular to both the photolysis and probe lasers using a quartz lens. The collected light was then transmitted through a series of optical filters, namely, FF01-315/15-25 (Semrock), UG11 (Schott), and FF02-320/40-25 (Semrock). Finally, the fluorescence was detected using a photomultiplier tube (PMT, Electron PDM9111-CP-TTL), and the signal was recorded by a multichannel scaler (Ortec MCS-PCI).

At a total pressure of 10 Torr, the concentrations of CH_2I_2 and CH_2OO were 4.0×10^{14} and 4.9×10^{12} cm^{-3}, respectively. The concentrations of CH_3CHI_2 and *syn*-CH_3CHOO were 5.0×10^{13} and 1.2×10^{12} cm^{-3}, respectively. Detailed calculation is provided in the Supporting Information. The concentration of acetaldehyde was varied from 0 to 2.90×10^{14} cm^{-3} for reaction 1 and from 0 to 5.96×10^{15} cm^{-3} for reaction 2.

We employed eq 1 to model the time-resolved profiles of the OH ($v'' = 0$, $N'' = 1$) signal generated from reaction 1.[4] An analogous modeling approach for the *syn*-CH_3CHOO reactions (reaction 2) is provided in the Supporting Information, including a detailed description of the indexing and derivation procedures.

$$S_{OH}(t) = \frac{A_0(k_3 + k_1' + k_4')}{(k_3 + k_1' + k_4')\, e^{(k_3+k_1'+k_4')t} + 2k_5[CH_2OO]_0[e^{(k_3+k_1'+k_4')t} - 1]} - A_1\, e^{-k_6't} \quad (3)$$

where

$$A_0 = \gamma \frac{k_{3a}[CH_2OO]_0}{k_6' - (k_3 + k_1' + k_4')}$$

and

$$A_1 = \gamma \left(\frac{k_{3a}[CH_2OO]_0}{k_6' - (k_3 + k_1' + k_4')} - [OH]_0 \right)$$

$k_1' = k_1[CH_3CHO]$, $k_4' = k_4[X]$, and $k_6' = k_6[Y]$.

The OH concentration originating from the decomposition of CH_2OO is represented by $[OH]_0$, while $[CH_2OO]_0$ denotes the initial concentration of CH_2OO, which was determined

https://doi.org/10.1021/acs.jpca.4c01374
J. Phys. Chem. A 2024, 128, 4956−4965

based on $[CH_2I_2]$ (further details are provided in the Supporting Information). The detection efficiency of OH is symbolized by γ. The unimolecular reaction rate of CH_2OO is represented by k_3, and k_{3a} specifically refers to the formation rate of OH from the unimolecular reaction of CH_2OO. The bimolecular reaction rate of CH_2OO with species present in the reaction cell—such as CH_2I_2 and I atoms—excluding CH_3CHO and CH_2OO, is denoted by k_4'. The self-reaction rate coefficient of CH_2OO is represented by k_5, and k_6' signifies the total consumption rate of OH, resulting from reactions of OH with various species, including CH_2I_2 and CH_3CHO. During the fitting process of OH signals, the parameters A_0, A_1, $k_3 + k_1' + k_4'$, and k_6' were treated as local parameters and allowed to vary. The self-reaction rate coefficient of CH_2OO, on the other hand, was considered a global parameter and fixed at a value of 8×10^{-11} cm^3 $molecule^{-1}$ s^{-1} according to the result of Ting et al.[40]

3. RESULTS AND DISCUSSION

3.1. OH Time-Resolved Profiles. Figure 1 shows the time-dependent OH profiles for the bimolecular reactions of CH_2OO and *syn*-CH_3CHOO with CH_3CHO at 298 K, with total pressures of 50 and 30 Torr for reactions 1 and 2, respectively. To vary the acetaldehyde concentration while maintaining a constant total flow rate, the flow rates of acetaldehyde and argon were adjusted simultaneously. The experimental data were fitted using eq 1 (eq S1 for reaction 2) with First Optimization software (1stOpt 7.0, 7D-soft High Technology Inc.), represented by the solid lines. The variation in the magnitude of the OH peak signal with the initial concentration of acetaldehyde was attributed to the reaction of OH with CH_3CHO and the difference in quenching cross sections of $OH(A^2\Sigma^+)$ by CH_3CHO and Ar. It is important to note that the reaction of OH with CH_3CHO does not affect the measurement of the rate coefficients for reactions 1 and 2 as this reaction is accounted for in the kinetic model (reactions 6 and 12) describing the OH time-dependent profile.

As k_6' (k_{12}') is larger than $k_3 + k_1' + k_4'$ ($k_9 + k_2' + k_{10}'$), as shown in Table S6 in the Supporting Information, the rise in the OH profile represents the OH loss kinetics, while the decay in the OH profile represents the OH formation kinetics, which originates from the unimolecular reactions of CH_2OO (*syn*-CH_3CHOO). Consequently, the decay of the OH profile represents the consumption of CH_2OO and *syn*-CH_3CHOO. By fitting the OH ($v'' = 0$) profiles with eq 1, $k_3 + k_1' + k_4'$ can be obtained. The value of k_1' is determined by subtracting ($k_3 + k_4'$), the intercept in the plots of $k_3 + k_1' + k_4'$ against $[CH_3CHO]$, from $k_3 + k_1' + k_4'$. The bimolecular rate coefficients k_1 and k_2, for the CH_2OO/*syn*-CH_3CHOO + CH_3CHO reactions, are obtained from the slopes of the linear fits of k_1' and k_2' vs $[CH_3CHO]$, as shown in the inset of Figure 1A,B.

3.2. Pressure-Dependent Rate Coefficients. The rate coefficients of reaction 1 (k_1) were measured at a temperature of 298 K and over a pressure range from 5.5 to 100 Torr. Figure 2 shows that the rate coefficient of reaction 1 (k_1) at 5.5 Torr is smaller compared to those measured between 10 and 100 Torr, within which no significant pressure dependence was observed. Table S1 in the Supporting Information provides comprehensive details regarding the pressure-dependent experimental conditions.

According to the findings of Elsamra et al.,[33] this reaction involves two submerged transition states (TS). The loose outer

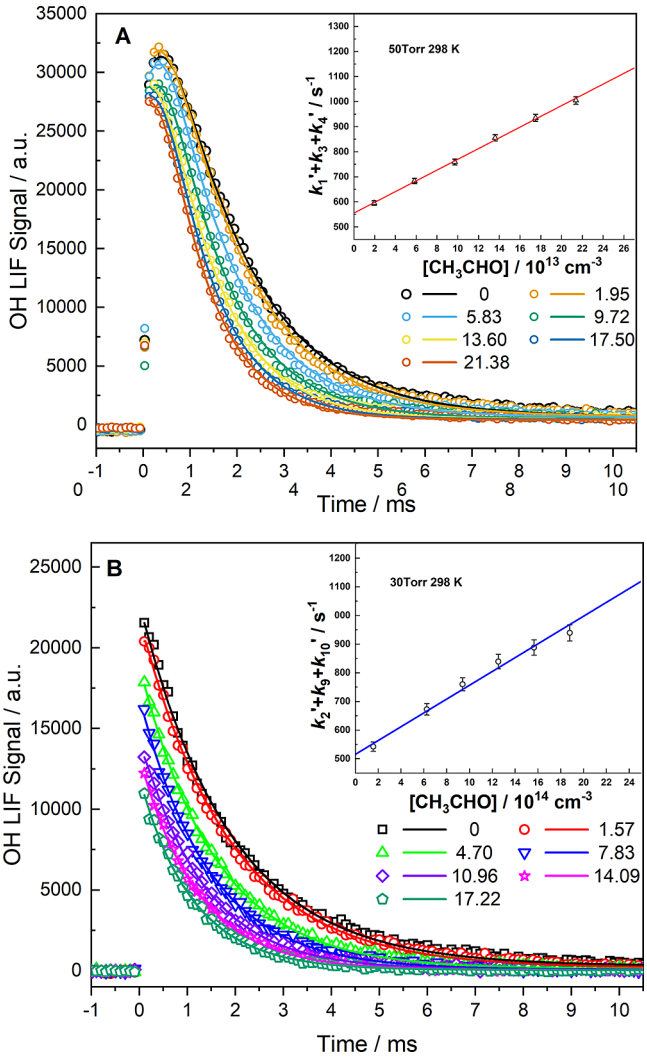

Figure 1. Typical time-dependent profiles of the OH signal for the CH_3CHO reaction with CH_2OO at 50 Torr (Figure 1A) and with *syn*-CH_3CHOO at 30 Torr (Figure 1B). The fits of the original data points (dots) with eqs 1 and S1 (shown in the Supporting Information) are shown in solid lines. The total loss rate of CH_2OO ($k_3 + k_1' + k_4'$) and *syn*-CH_3CHOO ($k_9 + k_2' + k_{10}'$) as a function of $[CH_3CHO]$ is shown in the insets. Error bars represent the total experimental error (for details, see the Supporting Information). Data from the above figures are listed in Tables S1 and S3 in the Supporting Information.

TS (TS_{outer}) separates the reactants and the van der Waals (VdW) complex, while the submerged inner TS (TS_{inner}) lies between the VdW complex and the reaction product. Consequently, the reaction can either proceed directly to the reaction products or traverse through the TS_{outer} to form the VdW complex, followed by either redissociation back to the reactants or crossing the TS_{inner} to yield the reaction products. The former route, where TS_{inner} is inaccessible, corresponds to the collisionless low-pressure limit process. It is worth noting that, as demonstrated by the theoretical calculations of Elsamra et al.,[33] the reaction remains in the low-pressure limit regime even at pressures extending up to thousands of Torr, where the rate coefficient exhibits minimal variation. The rate coefficients obtained in the present study are, therefore, the low-pressure limit values, which are in good accordance with the calculated

https://doi.org/10.1021/acs.jpca.4c01374
J. Phys. Chem. A 2024, 128, 4956−4965

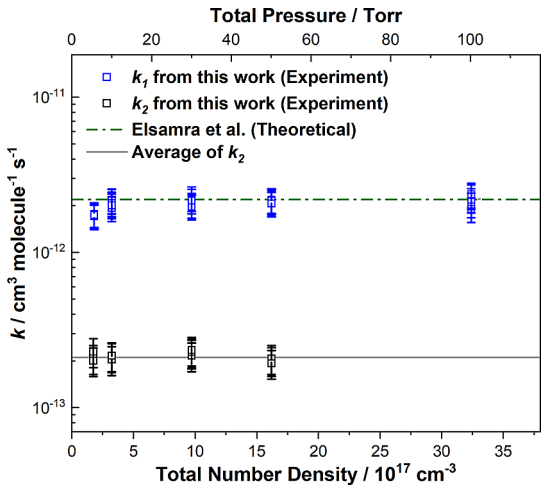

Figure 2. Measured rate coefficients for CH_2OO and *syn*-CH_3CHOO reactions with CH_3CHO at 298 K and various pressures. The error bar of each rate coefficient includes all experimental errors. The gray line shows the average value of k_2.

rate coefficients reported by Elsamra et al., except for a smaller value observed at 5.5 Torr, as depicted in Figure 2.

Figure 2 demonstrates that the reaction of *syn*-CH_3CHO with CH_3CHO exhibits no significant dependence on pressure. By calculating the average of the measured values of k_2 over a pressure range of 5−50 Torr, we obtained a rate coefficient of $(2.11 \pm 0.45) \times 10^{-13}$ cm^3 molecule^{-1} s^{-1} at 298 K. This value is approximately 1 order of magnitude smaller than that of the CH_2OO + CH_3CHO reaction. Measurements of rate coefficients at pressures exceeding 50 Torr were not conducted due to the substantial collisional quenching of OH ($A^2\Sigma^+$) by species such as CH_3CHO and Ar. It is important to note that the concentration of CH_3CHO in reaction 2 is roughly an order of magnitude higher than in reaction 1, which can be attributed to the low reactivity of the former reaction. The average values of k_2 are presented in Table 1, and detailed data

Table 1. Summary of Rate Coefficients for Reaction 2 (k_2) at 298 K and Different Pressures[a]

pressure (Torr)	$k_2/10^{-13}$[b] (cm^3 molecule^{-1} s^{-1})
5.3	2.12 ± 0.45
10	2.12 ± 0.45
30	2.20 ± 0.46
50	2.01 ± 0.42

[a]For details, see Table S3 in the Supporting Information. [b]The average value of the rate coefficient from measurements at the same pressure.

on the experimental conditions can be found in Table S3 (Supporting Information). The absence of pressure dependence in the reaction of *syn*-CH_3CHOO with CH_3CHO may be explained by the fact that the VdW complex possesses more molecular degrees of freedom compared to the CH_2OO reaction with CH_3CHO. Consequently, the trend in rate coefficients versus pressure for the *syn*-CH_3CHOO reaction resembles that of the CH_2OO reaction at higher pressure. This observation is consistent with the calculated result by Jalan et al. for the reaction of CH_2OO with CH_3CHO, C_2H_5CHO, and CH_3COCH_3, which indicate that the onset of high-pressure behavior shifts to lower pressure as the molecular degrees of freedom increase.[19]

The substitution of a methyl group for the H atom in CH_2OO, yielding *syn*-CH_3CHOO, generates substantial steric hindrance, thereby slowing down the reaction rates of *syn*-CH_3CHOO compared to that of CH_2OO. Moreover, the increased substitution can also influence the reaction barrier, either reducing it (e.g., in reactions with alkenes[41]) or increasing it (e.g., in reactions with NH_3[42]). This modulation of the reaction barrier can either counteract or synergize with the effects of steric hindrance, ultimately leading to varying reactivity ratios between *syn*-CH_3CHOO and CH_2OO in bimolecular reactions. When reacting with CH_3CHO, it is likely that both the steric hindrance effect and the increased reaction barrier (as indicated by the activation energy values provided in section 3.4) contribute to the slower reaction rate of *syn*-CH_3CHOO compared to that of CH_2OO with CH_3CHOO.

3.3. Comparison with Previous Results and the Effect of Bath Gas. The average values of k_1 at various pressures, along with previous experimental findings, are presented in Figure 3 and Table 2. The rate coefficient from the current

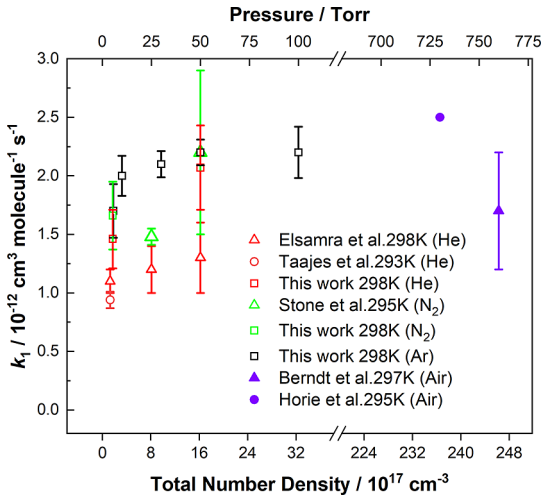

Figure 3. Comparison of rate coefficients measured at different pressures and with different bath gases.

experiment exhibits pressure dependence, a trend consistent with previous experimental results.[32,33] Our result at 50 Torr agrees with the value reported by Stone et al.[32] at the same pressure, which was measured using the laser-induced fluorescence method by detecting the HCHO product. It also aligns with the value obtained by Berndt et al.[43] at 760 Torr, measured in a free-jet flow system with a chemical ionization-atmospheric pressure interface time-of-flight mass spectrometer. Our experimental result at a pressure of 30 Torr, yielding a rate coefficient of $(2.10 \pm 0.38) \times 10^{-12}$ cm^3 molecule^{-1} s^{-1}, is larger than the values reported by Stone et al. ($(1.48 \pm 0.04) \times 10^{-12}$ cm^3 molecule^{-1} s^{-1})[32] and Elsamra et al. ($(1.2 \pm 0.2) \times 10^{-12}$ cm^3 molecule^{-1} s^{-1})[33] at a lower pressure of 25 Torr, with the latter determined utilizing the multiple-pass UV absorption technique. At lower pressure, the rate coefficient we measured at 5.5 Torr is consistent with that measured by Taatjes et al.[31] at 4 Torr using a multiplexed photoionization mass spectrometer, considering the experimental uncertainty.

https://doi.org/10.1021/acs.jpca.4c01374
J. Phys. Chem. A 2024, 128, 4956−4965

Table 2. Summary of Rate Coefficients (k_1) for Reaction 1

k_1/ 10^{-12} (cm^3 $molecule^{-1}$ s^{-1})	P/ Torr	temp./K	bath gas	technique	ref
0.95 ± 0.07	4	293	He	PLP−PIMS	Taatjes et al.[31]
1.48 ± 0.04	25	295	N_2	PLP-LIF/ PIMS	Stone et al.[32]
~2.2	50				
1.7 ± 0.5	760	297	air	free-jet FR-TOF-MS	Berndt et al.[43]
1.1 ± 0.1	4	298	He	PLP-UV abs.	Elsamra et al.[33]
1.2 ± 0.2	25				
1.3 ± 0.2	50				
1.73 ± 0.32	5.5	298	Ar	PLP-LIF	this work
2.08 ± 0.38	10				
2.10 ± 0.38	30				
2.13 ± 0.38	50				
2.16 ± 0.39	100				
~2.5	730	295	air	FTIR	Horie et al.[18]

It is worth noting that previous experiments on the rate coefficient measurement for the CH_2OO reaction with CH_3CHO were conducted using different bath gases, and some of the previous experimental results are smaller than ours, especially at pressures below 25 Torr. Consequently, we investigated the influence of bath gas on the rate coefficient of this reaction at 298 K and 5.4−50 Torr. As shown in Figure 4A, at 5.4 Torr, the slope from the linear fit obtained with He as the bath gas is noticeably smaller than those obtained with Ar and N_2 (1.46 vs 1.66−1.73 × 10^{-12} cm^3 $molecule^{-1}$ s^{-1}), indicating that He is less effective than Ar and N_2 in relaxing the VdW complex. The corresponding rate coefficients are listed in Table 3. This observation suggests that the use of different bath gases and slight pressure differences might contribute to the smaller rate coefficient measured by Taatjes et al. at 4 Torr compared to our result at 5.5 Torr. At 50 Torr and 298 K, the rate coefficients measured with He and Ar as the bath gas are similar. The rate coefficients measured with different bath gases, averaged from several sets of measurements, are listed in Table 3, and the results from each set of measurements are provided in the Supporting Information (Table S7 and Figure S2).

Table 3. Summary of the Rate Coefficient of Reaction 1 (k_1) Measured with Different Bath Gases at 298 K[a]

bath gas	pressure (Torr)	$k_1/10^{-12}$[b] (cm^3 $molecule^{-1}$ s^{-1})
Ar	5.4	1.73 ± 0.30
N_2	5.3	1.66 ± 0.29
He	5.3	1.46 ± 0.25
Ar	50	2.14 ± 0.37
He	50	2.07 ± 0.36

[a]For details, see Table S7 in the Supporting Information. [b]The average value of the rate coefficient from measurements at the same pressure.

3.4. Temperature-Dependent Rate Coefficients. The effective loss rates of CH_2OO and *syn*-CH_3CHOO reactions with CH_3CHO were measured at four different temperatures from 280 to 333 K, and the results were plotted against [CH_3CHO], as shown in Figure 5. The steeper gradients observed at lower temperatures suggest that the rate coefficients of reaction 1 exhibit a negative temperature dependence. By averaging the k_1 values obtained from various sets of measurements at each temperature, the rate coefficients were determined to be (2.57 ± 0.46), (2.13 ± 0.38), (1.80 ± 0.33), and (1.56 ± 0.28) × 10^{-12} cm^3 $molecule^{-1}$ s^{-1} at 50 Torr and temperatures of 280, 298, 318, and 333 K, respectively. The detailed data can be found in Table S2 of the Supporting Information. Conversely, Figure 5B reveals a positive temperature dependence for the *syn*-CH_3CHOO reaction with CH_3CHO. The averaged rate coefficients, k_2, were found to be (1.92 ± 0.41), (2.26 ± 0.48), (2.86 ± 0.60), and (3.62 ± 0.76) × 10^{-13} cm^3 $molecule^{-1}$ s^{-1} at 30 Torr and temperatures of 283, 298, 313, and 333 K, respectively. Additional temperature-dependent experiments were conducted at 10 Torr, yielding rate coefficients consistent with those obtained at 30 Torr. The details of the experimental data and conditions for both 30 and 10 Torr are provided in Tables S4 and S5 of the Supporting Information.

Figure 6 presents the Arrhenius logarithmic plots of the temperature-dependent rate coefficients for the CH_2OO/*syn*-

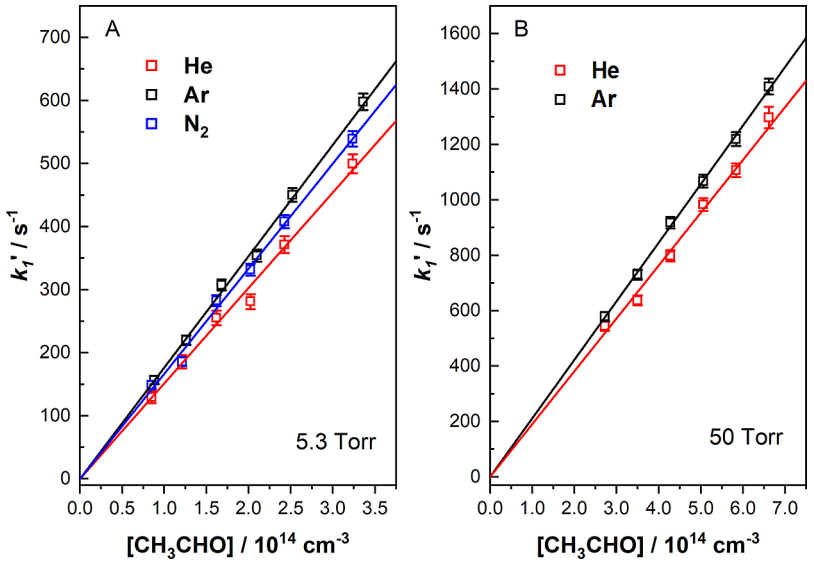

Figure 4. (A, B) Effective loss rate k_1' as a function of [CH_3CHO] with He, Ar, and N_2 as bath gases at 5.3 and 50 Torr.

https://doi.org/10.1021/acs.jpca.4c01374
J. Phys. Chem. A 2024, 128, 4956−4965

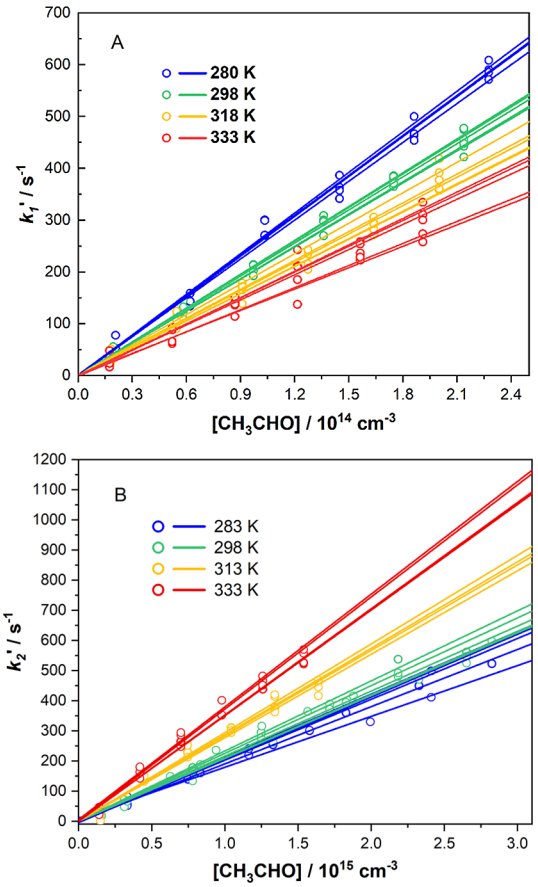

Figure 5. (A, B) Effective loss rate k_1' as a function of [CH_3CHO] at 50 Torr and four different temperatures. The slopes of the linear fits give the bimolecular rate coefficients for the CH_2OO/*syn*-CH_3CHOO + CH_3CHO reaction at each temperature.

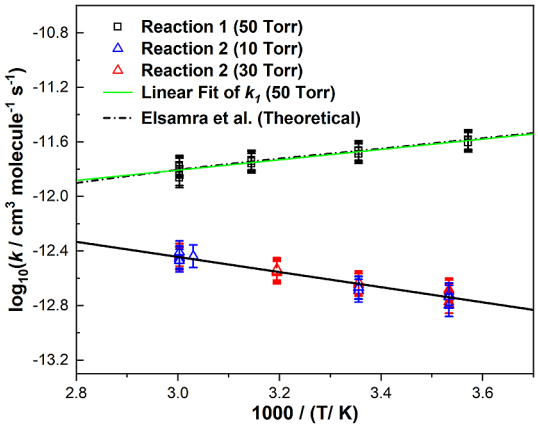

Figure 6. Arrhenius logarithmic plot of the measured rate coefficients of reactions 1 and 2. The black rectangular hollow points are experimental data of reaction 1 at 50 Torr, and the green line is the linear fit to the logarithmic plot. The black dashed line is the theoretical result adopted by Elsamra et al.[33] The red and blue triangular hollow points are experimental data of reaction 2 at 30 and 10 Torr, respectively. The black line is the linear fit to the logarithmic plot. The error bar represents the total experimental errors.

CH_3CHOO reaction with CH_3CHO. The green and black lines represent the fit of $\log_{10}(k_1)$ and $\log_{10}(k_2)$ using the Arrhenius equation, $k(T) = A\exp(-E_a/RT)$. The temperature-dependent rate coefficients, $k_1(T)$ and $k_2(T)$, can be expressed as follows:

$$k_1(T) = (1.15 \pm 0.21) \times 10^{-13}\ \text{cm}^3\ \text{molecule}^{-1}\ \text{s}^{-1} \cdot\exp[(1.73 \pm 0.31)\ \text{kcal mol}^{-1}/RT]$$

$$k_2(T) = (1.66 \pm 0.61) \times 10^{-11}\ \text{cm}^3\ \text{molecule}^{-1}\ \text{s}^{-1} \cdot\exp[(-2.32 \pm 0.49)\ \text{kcal mol}^{-1}/RT]$$

Previous calculations suggested that the current experiment on the reaction of CH_2OO with CH_3CHO proceeded under low-pressure limit conditions.[33] As shown in Figure 6, the temperature-dependent rate coefficients obtained from our experiment align well with the calculated values. The activation energy determined from the current experiment is consistent with the theoretical value, accounting for experimental uncertainties. However, the pre-exponential factor is smaller than the theoretical value, as indicated in Table 4. In contrast, previous experimental results (298−500 K)[33] showed rate coefficients approximately half of the calculated value but demonstrated a closer match better with the theoretical activation energy and pre-exponential factor. It should be noted that the theoretical pre-exponential factor and activation energy were derived from rate coefficients over a wider temperature range (approximately 270−550 K), and the Arrhenius plot does not exhibit a strictly linear relationship.

Table 4. Arrhenius Parameters for the CH_2OO Reaction with CH_3CHO

parameters[a]	this work (P = 50 Torr in Ar)	theory[b] (P = 0)	experiment (P = 25 Torr in He)
A	$(1.15 \pm 0.21) \times 10^{-14}$	6.6×10^{-14}	$(3 \pm 0.8) \times 10^{-14}$
E_a	-1.73 ± 0.31	-2.1	-2.2 ± 0.6

[a]In units of A: cm^3 molecule^{-1} s^{-1} and E_a: kcal mol^{-1}. [b]Low-pressure limit values, ref 33.

The negative temperature dependence of reaction 1 is attributed to the presence of submerged transition state barriers between the VdW complex and reaction products, while the positive temperature dependence of reaction 2 suggests the existence of a positive barrier along the reaction coordinate. It is worth noting that the reaction of *syn*-CH_3CHOO with acrolein exhibits negative temperature dependence, despite having a similar room-temperature rate coefficient of $(1.17 \pm 0.16) \times 10^{-13}$ cm^3 molecule^{-1} s^{-1} to the current reaction.[44] These results suggest that the rate coefficients for reactions between *syn*-CIs and aldehydes are likely to be on the order of 10^{-13} cm^3 molecule^{-1} s^{-1}. Furthermore, the energy barrier along the reaction coordinate is expected to be relatively low, approximately 1−2 kcal mol^{-1} above or below the energy of the reactants. This expectation is based on the measured value of 2.32 ± 0.49 kcal mol^{-1} for the *syn*-CH_3CHOO reactions with acetaldehyde and the reported value of -1.47 ± 0.24 kcal mol^{-1} for the *syn*-CH_3CHOO reactions with acrolein.[45] In contrast, CH_2OO is expected to be a more representative model for *anti*-CIs.

Among the cycloaddition reactions of *anti*- and *syn*-CH_3CHOO, their reactions with CO_2 exhibit a strong conformer dependence, with the rate coefficients differing by 4 orders of magnitude.[46] In contrast, their reactions with SO_2 display a relatively modest conformer dependence, with the

https://doi.org/10.1021/acs.jpca.4c01374
J. Phys. Chem. A 2024, 128, 4956−4965

rate coefficients differing by a factor of 2.5−7.6.[8,10,11,13,35,47] Although a direct comparison is not possible due to the lack of theoretical or experimental results on the *anti*-CH_3CHOO reaction with CH_3CHO, the reactivity of CH_2OO and *syn*-CH_3CHOO with CH_3CHO differs by an order of magnitude, indicating that the reactions between *syn*-/*anti*-CH_3CHOO and CH_3CHO are unlikely to be strongly conformer-dependent.

4. ATMOSPHERIC IMPLICATIONS

Acetaldehyde, together with formaldehyde and acetone, is one of the top three carbonyl compounds emitted by certain plant species.[30] Formaldehyde and acetaldehyde typically have the highest ambient concentrations among all carbonyl compounds.[48−50] Acetaldehyde removal in the atmosphere is dominated by the reaction with OH radicals and solar photolysis.[28] The oxidation of aldehydes by OH forms acyl radicals, which react with O_2 to form acyl peroxy radicals and RO_2 radicals,[51,52] which participate in the atmospheric NO_X cycle and impact O_3 formation.[53,54]

The ratios of the consumption rates of CH_3CHO by CH_2OO vs OH and *syn*-CH_3CHOO vs OH are calculated according to eqs 4 and 5.

$$v_1 = \frac{k_1[CH_2OO][CH_3CHO]}{k_{OH}[OH][CH_3CHO]} = \frac{k_1[CH_2OO]}{k_{OH}[OH]} \quad (4)$$

$$v_2 = \frac{k_2[syn\text{-}CH_3CHOO][CH_3CHO]}{k_{OH}[OH][CH_3CHO]} = \frac{k_2[syn\text{-}CH_3CHOO]]}{k_{OH}[OH]} \quad (5)$$

In eqs 4 and 5, k_1 and k_2 represent the bimolecular rate coefficients of *R*1 and *R*2 observed in the present work, while k_{OH} denotes the bimolecular rate coefficient for the reaction of OH + CH_3CHO, given by[28]

$$k_{OH}(T) = (5.32 \pm 0.55) \times 10^{-12} \exp[(315 \pm 40)/T] \ cm^3\ molecule^{-1}\ s^{-1}$$

The typical concentration of OH radicals ranges from 10^4 to 10^6 cm^{-3},[55−60] with a global tropospheric concentration approximately 8.8×10^5 cm^{-3}. In calculations with eqs 2 and 3, we fixed [OH] to 8.8×10^5 cm^{-3}. Atmospheric concentrations of CIs are estimated to be between 10^4 and 10^5 cm^{-3}.[61,62] Therefore, as shown in Figure 7, [CH_2OO] and [*syn*-CH_3CHOO] were varied from 0 to 1×10^5 cm^{-3}.

Figure 7A shows that the consumption rate of CH_3CHO by CH_2OO is about 2 to 4 orders slower than by OH at temperatures between 200 and 330 K. Similarly, the consumption rate of CH_3CHO by *syn*-CH_3CHOO is about 3 to 5 orders slower than by OH, as shown in Figure 7B. At a concentration as high as 1×10^5 cm^{-3} for CH_2OO and *syn*-CH_3CHOO, CH_3CHO degradation by CH_2OO and *syn*-CH_3CHOO accounts for about 3.9 and 0.28%, respectively, compared to that by OH. This observation is in accord with prior research[23] that reactions with CIs constitute a relatively insignificant atmospheric sink for acetaldehyde, as compared to reactions with OH or photolytic degradation pathways.

5. CONCLUSIONS

In this work, the rate coefficients for the reaction of CH_2OO and *syn*-CH_3CHOO with CH_3CHO were investigated at various temperatures and pressures using a laser-induced fluorescence technique to monitor the temporal profiles of OH($v'' = 0$). For the reaction of CH_2OO with CH_3CHO, the rate coefficient at 5.5 Torr was found to be smaller than those between 10 and 100 Torr. At low pressure (~5.3 Torr), the choice of bath gas influenced the rate coefficient, with He yielding a smaller value compared to Ar and N_2. However, at 50 Torr and 298 K, the rate coefficients were similar for all bath gases, with a value of $(2.13 \pm 0.39) \times 10^{-12}$ cm^3 $molecule^{-1}$ s^{-1} when using Ar as the bath gas. This reaction exhibited a negative temperature dependence between 280 and 333 K, with an activation energy of (-1.73 ± 0.31) kcal mol^{-1}. The rate coefficients obtained in this study are consistent with most previously reported experimental results and theoretical calculations.

For the reaction of *syn*-CH_3CHOO with CH_3CHO, no significant pressure dependence was observed for the rate coefficient over the range of 5−50 Torr, and the bimolecular rate coefficient was determined to be $(2.11 \pm 0.45) \times 10^{-13}$ cm^3 $molecule^{-1}$ s^{-1}. In contrast to CH_2OO with the CH_3CHO reaction, this reaction showed a positive temperature dependence between 283 and 333 K, with an activation energy of (2.32 ± 0.49) kcal mol^{-1}.

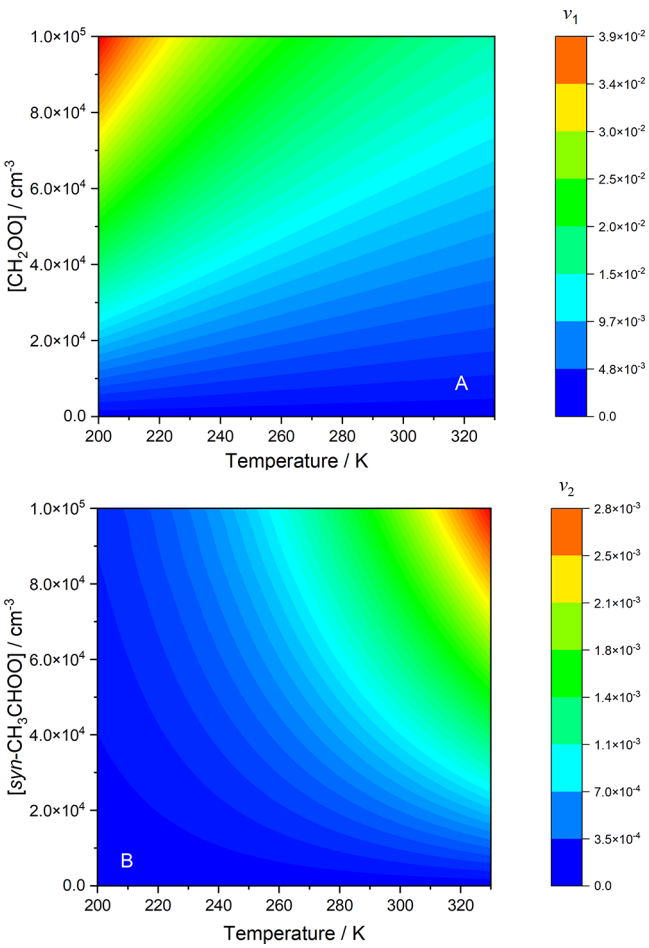

Figure 7. Rate ratios v_1 and v_2 as a function of temperature (200−330 K) are shown for two cases: (A) varying CH_2OO concentration and (B) varying *syn*-CH_3CHOO concentration.

https://doi.org/10.1021/acs.jpca.4c01374
J. Phys. Chem. A 2024, 128, 4956−4965

■ ASSOCIATED CONTENT

Supporting Information

The Supporting Information is available free of charge at https://pubs.acs.org/doi/10.1021/acs.jpca.4c01374.

Error analysis; kinetic model for the title reactions; UV absorption spectroscopy of acetaldehyde; summary of experimental conditions; and effect of bath gases (PDF)

■ AUTHOR INFORMATION

Corresponding Author

Wenrui Dong − *State Key Laboratory of Molecular Reaction Dynamics, Dalian Institute of Chemical Physics, Chinese Academy of Sciences, Dalian 116023, China; Hefei National Laboratory, Hefei 230088, China;* orcid.org/0000-0002-3640-1821; Email: wrdong@dicp.ac.cn

Authors

Haotian Jiang − *Department of Chemical Physics, School of Chemistry and Materials Science, University of Science and Technology of China, Hefei 230026, China; State Key Laboratory of Molecular Reaction Dynamics, Dalian Institute of Chemical Physics, Chinese Academy of Sciences, Dalian 116023, China;* orcid.org/0000-0001-9764-4029

Yue Liu − *Department of Chemical Physics, School of Chemistry and Materials Science, University of Science and Technology of China, Hefei 230026, China; State Key Laboratory of Molecular Reaction Dynamics, Dalian Institute of Chemical Physics, Chinese Academy of Sciences, Dalian 116023, China*

Chunlei Xiao − *Department of Chemical Physics, School of Chemistry and Materials Science, University of Science and Technology of China, Hefei 230026, China; State Key Laboratory of Molecular Reaction Dynamics, Dalian Institute of Chemical Physics, Chinese Academy of Sciences, Dalian 116023, China; Hefei National Laboratory, Hefei 230088, China;* orcid.org/0000-0002-1549-5945

Xueming Yang − *State Key Laboratory of Molecular Reaction Dynamics, Dalian Institute of Chemical Physics, Chinese Academy of Sciences, Dalian 116023, China; Department of Chemistry, Southern University of Science and Technology, Shenzhen 518055, China;* orcid.org/0000-0001-6684-9187

Complete contact information is available at: https://pubs.acs.org/10.1021/acs.jpca.4c01374

Notes

The authors declare no competing financial interest.

■ ACKNOWLEDGMENTS

The authors gratefully acknowledge the Dalian Coherent Light Source (DCLS) for support and assistance. This work was funded by the National Natural Science Foundation of China (NSFC No. 22288201), the Chinese Academy of Sciences (GJJSTD20220001), and the Innovation Program for Quantum Science and Technology (No. 2021ZD0303305).

■ REFERENCES

(1) Criegee, R. Mechanism of Ozonolysis. *Angewandte Chemie International Edition in English* **1975**, *14* (11), 745−752.

(2) Lewis, T. R.; Blitz, M. A.; Heard, D. E.; Seakins, P. W. Direct evidence for a substantive reaction between the Criegee intermediate, CH2OO, and the water vapour dimer. *Phys. Chem. Chem. Phys.* **2015**, *17* (7), 4859−4863.

(3) Lin, L. C.; Chang, H. T.; Chang, C. H.; Chao, W.; Smith, M. C.; Chang, C. H.; Lin, J. J. M.; Takahashi, K. Competition between H2O and (H2O)(2) reactions with CH2OO/CH3CHOO. *Phys. Chem. Chem. Phys.* **2016**, *18* (6), 4557−4568.

(4) Liu, Y.; Liu, F.; Liu, S.; Dai, D.; Dong, W.; Yang, X. A kinetic study of the CH(2)OO Criegee intermediate reaction with SO(2), (H(2)O)(2), CH(2)I(2) and I atoms using OH laser induced fluorescence. *Phys. Chem. Chem. Phys.* **2017**, *19* (31), 20786−20794.

(5) Anglada, J. M.; Sole, A. Impact of the water dimer on the atmospheric reactivity of carbonyl oxides. *Phys. Chem. Chem. Phys.* **2016**, *18* (26), 17698−17712.

(6) Long, B.; Bao, J. L.; Truhlar, D. G. Atmospheric Chemistry of Criegee Intermediates: Unimolecular Reactions and Reactions with Water. *J. Am. Chem. Soc.* **2016**, *138* (43), 14409−14422.

(7) Yin, C.; Takahashi, K. How does substitution affect the unimolecular reaction rates of Criegee intermediates? *Phys. Chem. Chem. Phys.* **2017**, *19* (19), 12075−12084.

(8) Taatjes, C. A.; Welz, O.; Eskola, A. J.; Savee, J. D.; Scheer, A. M.; Shallcross, D. E.; Rotavera, B.; Lee, E. P.; Dyke, J. M.; Mok, D. K.; et al. Direct measurements of conformer-dependent reactivity of the Criegee intermediate CH3CHOO. *Science* **2013**, *340* (6129), 177−180.

(9) Berndt, T.; Voigtlander, J.; Stratmann, F.; Junninen, H.; Mauldin, R. L., 3rd; Sipila, M.; Kulmala, M.; Herrmann, H. Competing atmospheric reactions of CH2OO with SO2 and water vapour. *Phys. Chem. Chem. Phys.* **2014**, *16* (36), 19130−19136.

(10) Sheps, L.; Scully, A. M.; Au, K. UV absorption probing of the conformer-dependent reactivity of a Criegee intermediate CH_3CHOO. *Phys. Chem. Chem. Phys.* **2014**, *16* (48), 26701−26706.

(11) Smith, M. C.; Ting, W. L.; Chang, C. H.; Takahashi, K.; Boering, K. A.; Lin, J. J. UV absorption spectrum of the C2 Criegee intermediate CH3CHOO. *J. Chem. Phys.* **2014**, *141* (7), 074302.

(12) Zou, M.; Liu, T.; Vansco, M. F.; Sojdak, C. A.; Markus, C. R.; Almeida, R.; Au, K.; Sheps, L.; Osborn, D. L.; Winiberg, F. A. F.; et al. Bimolecular Reaction of Methyl-Ethyl-Substituted Criegee Intermediate with SO(2). *J. Phys. Chem. A* **2023**, *127* (43), 8994−9002.

(13) Howes, N. U. M.; Mir, Z. S.; Blitz, M. A.; Hardman, S.; Lewis, T. R.; Stone, D.; Seakins, P. W. Kinetic studies of C(1) and C(2) Criegee intermediates with SO(2) using laser flash photolysis coupled with photoionization mass spectrometry and time resolved UV absorption spectroscopy. *Phys. Chem. Chem. Phys.* **2018**, *20* (34), 22218−22227.

(14) Chen, L.; Huang, Y.; Xue, Y.; Cao, J.; Wang, W. Competition between HO(2) and H(2)O(2) Reactions with CH(2)OO/anti-CH(3)CHOO in the Oligomer Formation: A Theoretical Perspective. *J. Phys. Chem. A* **2017**, *121* (37), 6981−6991.

(15) Newland, M. J.; Rickard, A. R.; Alam, M. S.; Vereecken, L.; Munoz, A.; Rodenas, M.; Bloss, W. J. Kinetics of stabilised Criegee intermediates derived from alkene ozonolysis: reactions with SO2, H2O and decomposition under boundary layer conditions. *Phys. Chem. Chem. Phys.* **2015**, *17* (6), 4076−4088.

(16) Green, A. M.; Barber, V. P.; Fang, Y.; Klippenstein, S. J.; Lester, M. I. Selective deuteration illuminates the importance of tunneling in the unimolecular decay of Criegee intermediates to hydroxyl radical products. *Proc. Natl. Acad. Sci. U. S. A.* **2017**, *114* (47), 12372−12377.

(17) Fang, Y.; Liu, F.; Barber, V. P.; Klippenstein, S. J.; McCoy, A. B.; Lester, M. I. Deep tunneling in the unimolecular decay of CH3CHOO Criegee intermediates to OH radical products. *J. Chem. Phys.* **2016**, *145* (23), 234308.

(18) Horie, O.; Schäfer, C.; Moortgat, G. K. High reactivity of hexafluoro acetone toward criegee intermediates in the gas-phase ozonolysis of simple alkenes. *International Journal of Chemical Kinetics* **1999**, *31* (4), 261−269.

(19) Jalan, A.; Allen, J. W.; Green, W. H. Chemically activated formation of organic acids in reactions of the Criegee intermediate with aldehydes and ketones. *Phys. Chem. Chem. Phys.* **2013**, *15* (39), 16841−16852.

(20) Kaipara, R.; Rajakumar, B. Temperature-Dependent Kinetics of the Reaction of a Criegee Intermediate with Propionaldehyde: A Computational Investigation. *J. Phys. Chem. A* **2018**, *122* (43), 8433−8445.
(21) Chhantyal-Pun, R.; Khan, M. A. H.; Martin, R.; Zachhuber, N.; Buras, Z. J.; Percival, C. J.; Shallcross, D. E.; Orr-Ewing, A. J. Direct Kinetic and Atmospheric Modeling Studies of Criegee Intermediate Reactions with Acetone. *ACS Earth and Space Chemistry* **2019**, *3* (10), 2363−2371.
(22) Wang, P. B.; Truhlar, D. G.; Xia, Y.; Long, B. Temperature-dependent kinetics of the atmospheric reaction between CH(2)OO and acetone. *Phys. Chem. Chem. Phys.* **2022**, *24* (21), 13066−13073.
(23) Cornwell, Z. A.; Harrison, A. W.; Murray, C. Kinetics of the Reactions of CH(2)OO with Acetone, alpha-Diketones, and beta-Diketones. *J. Phys. Chem. A* **2021**, *125* (39), 8557−8571.
(24) Debnath, A.; Rajakumar, B. Investigation of kinetics and mechanistic insights of the reaction of criegee intermediate (CH(2)OO) with methyl-ethyl ketone (MEK) under tropospherically relevant conditions. *Chemosphere* **2023**, *312* (Pt 1), No. 137217.
(25) Wang, J.; Chen, H.; Glass, G. P.; Curl, R. F. Kinetic Study of the Reaction of Acetaldehyde with OH. *J. Phys. Chem. A* **2003**, *107* (49), 10834−10844.
(26) Sivakumaran, V.; Crowley, J. N. Reaction between OH and CH3CHO. *Phys. Chem. Chem. Phys.* **2003**, *5* (1), 106−111.
(27) Taylor, P. H.; Yamada, T.; Marshall, P. The reaction of OH with acetaldehyde and deuterated acetaldehyde: Further insight into the reaction mechanism at both low and elevated temperatures. *International Journal of Chemical Kinetics* **2006**, *38* (8), 489−495.
(28) Zhu, L.; Talukdar, R. K.; Burkholder, J. B.; Ravishankara, A. R. Rate coefficients for the OH + acetaldehyde (CH3CHO) reaction between 204 and 373 K. *International Journal of Chemical Kinetics* **2008**, *40* (10), 635−646.
(29) Hui, A. O.; Okumura, M.; Sander, S. P. Temperature Dependence of the Reaction of Chlorine Atoms with CH(3)OH and CH(3)CHO. *J. Phys. Chem. A* **2019**, *123* (23), 4964−4972.
(30) Villanueva-Fierro, I.; Popp, C. J.; Martin, R. S. Biogenic emissions and ambient concentrations of hydrocarbons, carbonyl compounds and organic acids from ponderosa pine and cottonwood trees at rural and forested sites in Central New Mexico. *Atmos. Environ.* **2004**, *38* (2), 249−260.
(31) Taatjes, C. A.; Welz, O.; Eskola, A. J.; Savee, J. D.; Osborn, D. L.; Lee, E. P.; Dyke, J. M.; Mok, D. W.; Shallcross, D. E.; Percival, C. J. Direct measurement of Criegee intermediate (CH2OO) reactions with acetone, acetaldehyde, and hexafluoroacetone. *Phys. Chem. Chem. Phys.* **2012**, *14* (30), 10391−10400.
(32) Stone, D.; Blitz, M.; Daubney, L.; Howes, N. U.; Seakins, P. Kinetics of CH2OO reactions with SO2, NO2, NO, H2O and CH3CHO as a function of pressure. *Phys. Chem. Chem. Phys.* **2014**, *16* (3), 1139−1149.
(33) Elsamra, R. M. I.; Jalan, A.; Buras, Z. J.; Middaugh, J. E.; Green, W. H. Temperature- and Pressure-Dependent Kinetics of CH2OO + CH3COCH3 and CH2OO + CH3CHO: Direct Measurements and Theoretical Analysis. *International Journal of Chemical Kinetics* **2016**, *48* (8), 474−488.
(34) Fenske, J. D.; Hasson, A. S.; Ho, A. W.; Paulson, S. E. Measurement of Absolute Unimolecular and Bimolecular Rate Constants for CH3CHOO Generated by thetrans-2-Butene Reaction with Ozone in the Gas Phase. *J. Phys. Chem. A* **2000**, *104* (44), 9921−9932.
(35) Zhou, X.; Liu, Y.; Dong, W.; Yang, X. Unimolecular Reaction Rate Measurement of syn-CH(3)CHOO. *J. Phys. Chem. Lett.* **2019**, *10* (17), 4817−4821.
(36) Mössinger, J. C.; Shallcross, D. E.; Anthony Cox, R. UV−VIS absorption cross-sections and atmospheric lifetimes of CH2Br2, CH2I2 and CH2BrI. *Journal of the Chemical Society, Faraday Transactions* **1998**, *94* (10), 1391−1396.
(37) Roehl, C. M.; Burkholder, J. B.; Moortgat, G. K.; Ravishankara, A. R.; Crutzen, P. J. Temperature dependence of UV absorption cross sections and atmospheric implications of several alkyl iodides. *Journal of Geophysical Research: Atmospheres* **1997**, *102* (D11), 12819−12829.
(38) Schmitt, G.; Comes, F. J. Photolysis of Ch2I2 and 1,1-C2H4I2 at 300 nm. *J. Photochem.* **1980**, *14* (2), 107−123.
(39) Hogan, P.; Davis, D. D. Electronic quenching and vibrational relaxation of the OH (A 2Σ+, v′=1) state. *J. Chem. Phys.* **1975**, *62* (11), 4574−4576.
(40) Ting, W. L.; Chang, C. H.; Lee, Y. F.; Matsui, H.; Lee, Y. P.; Lin, J. J. Detailed mechanism of the CH(2)I + O(2) reaction: yield and self-reaction of the simplest Criegee intermediate CH(2)OO. *J. Chem. Phys.* **2014**, *141* (10), 104308.
(41) Vereecken, L.; Harder, H.; Novelli, A. The reactions of Criegee intermediates with alkenes, ozone, and carbonyl oxides. *Phys. Chem. Chem. Phys.* **2014**, *16* (9), 4039−4049.
(42) Misiewicz, J. P.; Elliott, S. N.; Moore, K. B.; Schaefer, H. F. Re-examining ammonia addition to the Criegee intermediate: converging to chemical accuracy. *Phys. Chem. Chem. Phys.* **2018**, *20* (11), 7479−7491.
(43) Berndt, T.; Kaethner, R.; Voigtlander, J.; Stratmann, F.; Pfeifle, M.; Reichle, P.; Sipila, M.; Kulmala, M.; Olzmann, M. Kinetics of the unimolecular reaction of CH2OO and the bimolecular reactions with the water monomer, acetaldehyde and acetone under atmospheric conditions. *Phys. Chem. Chem. Phys.* **2015**, *17* (30), 19862−19873.
(44) Zhou, X.; Chen, Y.; Liu, Y.; Li, X.; Dong, W.; Yang, X. Kinetics of CH(2)OO and syn-CH(3)CHOO reaction with acrolein. *Phys. Chem. Chem. Phys.* **2021**, *23* (23), 13276−13283.
(45) Zhou, X.; Chen, Y.; Liu, Y.; Li, X.; Dong, W.; Yang, X. Kinetics of CH2OO and syn-CH3CHOO reaction with acrolein. *Phys. Chem. Chem. Phys.* **2021**, *23* (23), 13276−13283.
(46) Lin, Y. H.; Takahashi, K.; Lin, J. J. Reactivity of Criegee Intermediates toward Carbon Dioxide. *J. Phys. Chem. Lett.* **2018**, *9* (1), 184−188.
(47) Lade, R. E.; Onel, L.; Blitz, M. A.; Seakins, P. W.; Stone, D. Kinetics of the Gas-Phase Reactions of syn- and anti-CH(3)CHOO Criegee Intermediate Conformers with SO(2) as a Function of Temperature and Pressure. *J. Phys. Chem. A* **2024**, *128* (14), 2815−2824.
(48) Liu, Q.; Gao, Y.; Huang, W.; Ling, Z.; Wang, Z.; Wang, X. Carbonyl compounds in the atmosphere: A review of abundance, source and their contributions to O3 and SOA formation. *Atmos. Res.* **2022**, *274*, No. 106184.
(49) Wang, H. K.; Huang, C. H.; Chen, K. S.; Peng, Y. P.; Lai, C. H. Measurement and source characteristics of carbonyl compounds in the atmosphere in Kaohsiung city. *Taiwan. J. Hazard Mater.* **2010**, *179* (1−3), 1115−1121.
(50) Geng, C.; Li, S.; Yin, B.; Gu, C.; Liu, Y.; Li, L.; Li, K.; Zhang, Y.; Azzi, M.; Li, H.; et al. Atmospheric Carbonyl Compounds in the Central Taklimakan Desert in Summertime: Ambient Levels, Composition and Sources. *Atmosphere* **2022**, *13* (5), 761.
(51) Zügner, G. L.; Szilágyi, I.; Zádor, J.; Szabó, E.; Dóbé, S.; Song, X.; Wang, B. OH yields for C2H5CO+O2 at low pressure: Experiment and theory. *Chem. Phys. Lett.* **2010**, *495* (4−6), 179−181.
(52) Tyndall, G. S.; Orlando, J. J.; Wallington, T. J.; Hurley, M. D.; Goto, M.; Kawasaki, M. Mechanism of the reaction of OH radicals with acetone and acetaldehyde at 251 and 296 K. *Phys. Chem. Chem. Phys.* **2002**, *4* (11), 2189−2193.
(53) Zhang, Y.; Xue, L.; Dong, C.; Wang, T.; Mellouki, A.; Zhang, Q.; Wang, W. Gaseous carbonyls in China's atmosphere: Tempo-spatial distributions, sources, photochemical formation, and impact on air quality. *Atmos. Environ.* **2019**, *214*, No. 116863.
(54) Wang, Y.; Guo, H.; Zou, S.; Lyu, X.; Ling, Z.; Cheng, H.; Zeren, Y. Surface O(3) photochemistry over the South China Sea: Application of a near-explicit chemical mechanism box model. *Environ. Pollut.* **2018**, *234*, 155−166.
(55) Ren, X. HOx concentrations and OH reactivity observations in New York City during PMTACS-NY2001. *Atmos. Environ.* **2003**, *37* (26), 3627−3637.
(56) Petäjä, T.; Mauldin, I. R. L.; Kosciuch, E.; McGrath, J.; Nieminen, T.; Paasonen, P.; Boy, M.; Adamov, A.; Kotiaho, T.;

Kulmala, M. Sulfuric acid and OH concentrations in a boreal forest site. *Atmos. Chem. Phys.* **2009**, *9* (19), 7435−7448.
(57) Stone, D.; Whalley, L. K.; Heard, D. E. Tropospheric OH and HO2 radicals: field measurements and model comparisons. *Chem. Soc. Rev.* **2012**, *41* (19), 6348−6404.
(58) Lelieveld, J.; Gromov, S.; Pozzer, A.; Taraborrelli, D. Global tropospheric hydroxyl distribution, budget and reactivity. *Atmospheric Chemistry and Physics* **2016**, *16* (19), 12477−12493.
(59) Li, M.; Karu, E.; Brenninkmeijer, C.; Fischer, H.; Lelieveld, J.; Williams, J. Tropospheric OH and stratospheric OH and Cl concentrations determined from CH4, CH3Cl, and SF6 measurements. *npj Clim. Atmos. Sci.* **2018**, *1* (1), 29.
(60) Kurylo, M. J.; Orkin, V. L. Determination of atmospheric lifetimes via the measurement of OH radical kinetics. *Chem. Rev.* **2003**, *103* (12), 5049−5076.
(61) Khan, M. A. H.; Percival, C. J.; Caravan, R. L.; Taatjes, C. A.; Shallcross, D. E. Criegee intermediates and their impacts on the troposphere. *Environ. Sci. Process Impacts* **2018**, *20* (3), 437−453.
(62) Novelli, A.; Hens, K.; Tatum Ernest, C.; Martinez, M.; Nölscher, A. C.; Sinha, V.; Paasonen, P.; Petäjä, T.; Sipilä, M.; Elste, T.; et al. Estimating the atmospheric concentration of Criegee intermediates and their possible interference in a FAGE-LIF instrument. *Atmospheric Chemistry and Physics* **2017**, *17* (12), 7807−7826.

https://doi.org/10.1021/acs.jpca.4c01374
J. Phys. Chem. A 2024, 128, 4956−4965